High-pressure homogenized citrus fiber cellulose dispersions

Structural characterization and flow behavior

Serial, M. R.; Velichko, E.; Nikolaeva, T.; den Adel, R.; Terenzi, C.; Bouwman, W. G.; van Duynhoven, J. P.M.

DOI
10.1016/j.foostr.2021.100237

Publication date
2021

Document Version
Final published version

Published in
Food Structure

Food Structure 30 (2021) 100237

Contents lists available at ScienceDirect

Food Structure

journal homepage: www.elsevier.com/locate/foostr

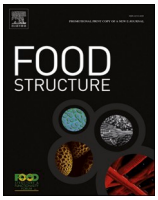

High-pressure homogenized citrus fiber cellulose dispersions: Structural characterization and flow behavior

M.R. Serial [a,1], E. Velichko [b,1], T. Nikolaeva [a], R. den Adel [c], C. Terenzi [a], W.G. Bouwman [b], J.P. M. van Duynhoven [a,c,*]

[a] Laboratory of Biophysics, Wageningen University & Research, Stippeneng 4, 6708WE, Wageningen, The Netherlands
[b] Department of Radiation Science & Technology, Delft University of Technology, Mekelweg 15, 2629JB Delft, The Netherlands
[c] Unilever Food Innovation Centre Hive, Bronland 14, 6708 WH, Wageningen, The Netherlands

ARTICLE INFO

Keywords:
Citrus fiber
cellulose
high-pressure homogenization
SAXS
rheo-MRI

ABSTRACT

Functionalized biomass waste sources of cellulose have drawn attention due to their high availability and sustainability properties. In this work we characterize the structural and flow properties of high-pressure homogenized citrus fiber cellulose dispersions, employing SAXS, rheology and rheo-MRI techniques. The high-pressure treatment disrupts the microfibrillar network within the citrus fibers, but leaves the individual microfibrils intact. Under moderate shear (0.1-100 s^{-1}) in a confined (< 1 mm) geometry, these functionalized citrus fiber cellulose dispersions exhibit thixotropic shear-banding behavior accompanied by cooperative flow of microfibril flocs with correlation lengths $\xi \sim$ 100 μm. The presented findings form a basis towards understanding and manipulating the structural and rheological properties of non-wood biomass cellulose microfibrils under industrially-relevant conditions.

1. Introduction

Environmental concerns and diminishing fossil resources are driving the development of renewable bio-based materials for the production of daily life products. Over the past few decades, cellulose micro- and nano-fibrils have gained significant interest due to their unique sustainable and biodegradable properties, with increasing applications ranging from protective coatings (Grüneberger, Künniger, Zimmermann, & Arnold, 2014) and packaging (Spence, Venditti, Rojas, Habibi, & Pawlak, 2010) to food and cosmetics (Klemm et al., 2018). Primary sources of cellulose are high fiber content biomass materials such wood or cotton, but also from non-wood sources such as wheat straw (Alemdar & Sain, 2008), potato tuber (Dufresne, Dupeyre, & Vignon, 2000) and banana rachis (Zuluaga et al., 2009). In the past years, more and more effort has been made on finding alternative sources of cellulose that ease the growing demand of wood-based raw materials and improve sustainability (Pennells, Godwin, Amiralian, & Martin, 2020; Yu et al., 2021). In this respect, citrus peel represents a valuable and sustainable source of cellulose since it contains large amounts of cellular structure and it represents a high percentage of food industry waste (Naz et al., 2016).

A promising route for functionalizing plant fibers is high-pressure homogenization (HPH) treatment. Recent studies performed on citrus fiber have shown that HPH treatment improves the functionality of citrus fibers, increasing water holding and texturing capacity as a result of enhanced swelling and network formation (Van Buggenhout et al., 2015; Willemsen et al., 2017; Willemsen, Panozzo, Moelants, Wallecan, & Hendrickx, 2020). However, the insight on the impact of HPH treatment at structural level is still limited, in particular at the sub-micron scale.

Many of the applications of HPH-treated cellulose fiber dispersions require the proper understanding of the relationship between microstructure and flow. Under shearing conditions, HPH-treated cellulose fiber dispersions are prone to exhibit shear-thinning and thixotropic behavior, arising from the formation and breakdown of shear-induced structures during flow (Nechyporchuk, Belgacem, & Pignon, 2016). In fact, flocculation dynamics has been addressed as the main cause of the complex rheological behavior of cellulose fiber dispersions. Such structural changes have been studied by means of digital imaging (Karppinen et al., 2012b; Saarikoski, Saarinen, Salmela, & Seppälä,

* Corresponding author.
E-mail address: John.vanDuynhoven@wur.nl (J.P.M. van Duynhoven).
[1] Equal contribution

https://doi.org/10.1016/j.foostr.2021.100237
Received 19 March 2021; Received in revised form 27 August 2021; Accepted 7 September 2021
Available online 26 October 2021

2012), ultrasonic speckle velocimetry (Martoïa et al., 2015), and rheo-MRI (de Kort et al., 2016), reporting shear-dependent flocs sizes in the range of (100 - 300 μm). Yet, only few studies focus on the impact of geometry dimensions on the observed flow behavior and structural properties of cellulose fiber suspensions during shear. This is particularly important when floc dimensions become comparable to the size of the geometry gap, as previously demonstrated elsewhere (de Kort et al., 2016; Saarikoski et al., 2012).

Here, we aim to explore the structural and flow properties of citrus fiber cellulose dispersions by means of SAXS and rheo-MRI techniques. In a first instance, we investigate the effect of both, HPH and concentration of fibers on the structural properties of citrus fiber dispersions. Following a systematic rheological characterization, we show that the flocculation dynamics on HPH-treated citrus fiber suspensions is affected by confined flow conditions, resulting in cooperative flow with correlation lengths in order of 100 μm.

The paper greatly benefited from a discussion of a preprint in the workshop Multiscale Simulations and Experimental Characterization of Foods, Wageningen, The Netherlands, 25 May- 27 May 2021 (M.R. Serial, 2021).

2. Materials and methods

2.1. Preparation of HPH treated citrus fiber suspensions

Citrus fiber dispersions were prepared by addition of Herbacel AQ+ type N from Herbafood Ingredients GmbH Germany (84−90% wt. dietary fiber, 4−9% wt. water, 2−5% wt. ash) to demineralized water at a 1 and 2% wt. concentration. The fibers were manufactured from citrus peels and contain 60% wt. cellulose, 3.4% wt. hemicellulose, and 5% wt. proteinaceous materials. Both citrus fiber dispersions were stirred using a Silverson (type L4RT-A) mixer at 4000 rpm for 10 minutes and subsequently pushed through a diamond coated Z-chamber (G10Z) of a high-pressure homogenizer (M-110S microfluidizer) at pressure of 300 - 1200 bar. The 1% wt. dispersion prepared at 1200 bar was pushed through the homogenizer multiple times. Ten samples of microbrillated citrus fiber were prepared by dilution of the 2% wt. suspension to various concentrations with demineralized water. A 0.08% wt. of Nipacide BIT 20 (Clariant) was added to all citrus fiber dispersions to prevent the material from degradation by microorganisms.

2.2. Confocal imaging

Confocal scanning laser microscopy (CSLM) was performed on a Leica TCS-SP5 confocal microscope. For all experiments, cellulose dispersions were stained by adding an aliquot of 0.5 w/v% Congo Red solution in water. Dyed samples were kept at room temperature for approximately one hour to reach equilibrium. For all images contrast was inverted for clarity purposes. Darker regions are associated to cellulose plant fibers whereas white represents the absence of fiber content.

2.3. Rheology

Flow curves of the microbrillated cellulose suspensions were measured on a stress-controlled rheometer (AR 2000, TA Instruments), using a plate-plate geometry (plate diameter 4 cm, gap 1 mm). During the measurements, the shear rate was first increased from 0.1 to 500 s^{-1} in 2 minutes and then decreased back to 0.1 s^{-1} in 2 min. Sand-blasted metal plates were used to prevent wall slip. All experiments were carried out at controlled temperature of 20 °C.

2.4. SAXS measurements

The high-brilliance ID02 beamline (Narayanan, Diat, & Bösecke, 2001) of the European Synchrotron Radiation Facility (ESRF) was employed for small-angle X-ray scattering measurements. Measurements were performed in a broad range of momentum transfers: $3 \times 10^{-4} \leq Q/Å \leq 0.7$, where $Q = 4\pi\lambda\, sin(2\theta)$ is the momentum transfer, θ is a scattering angle and λ the wavelength of the used X-rays (in our experiments $\lambda = 0.0996$ nm). The samples were placed in a 30 position temperature stage with aluminum sample holders between X-ray mica windows, at a constant temperature of the stage 20 °C. Scattering of 2 mm of water between two mica windows was used for a background subtraction for all the measurements. Water reference ($I_{H_2O,20°C} = 1.641\ 10^{-2}\ cm^{-1}$) was also used for scaling of the scattering intensities to absolute units [cm^{-1}].

The SAXS data were fitted using the SASview package (Doucet et al., 2018) and applying a two-level scattering model. The model consists of a cylinder form-factor of the cellulose fibrils with polydisperse radii, and a power-law function describing the agglomerates of the fibrils:

$$I(Q) = \frac{sf}{V}\sum_{R_{cyl}} n\left(R_{cyl}, \sigma_{R_{cyl}}\right)\cdot P\left(q, R_{cyl}, L, \rho_{cyl}, \rho_{solv}\right) + A\cdot q^{-m} \quad (1)$$

where the first term corresponds to the form factor of a cylinder with polydisperse radii (R_{cyl} – an average radius of cylinders, $\sigma_{R_{cyl}}$ – a standard deviation of the radius, q – momentum transfer, L – length of cylinders, ρ_{cyl}, ρ_{solv} – scattering length density of the cylinders and the solvent, respectively), multiplied by the number density of particles (sf/V), where V is the total volume of the particle, and the last term accounts for the power-law behavior of the network. The model is inspired by the one proposed and successfully applied by Martinez-Sanz et al. (Martínez-Sanz, Mikkelsen, Flanagan, Gidley, & Gilbert, 2016; Martínez-Sanz, Mikkelsen, Flanagan, Rehm, et al., 2016). However, since the X-ray scattering length densities for core and shell of the structure are quite similar (SLD core cellulose = $14.46{\cdot}10^{10}$ cm^{-2} and SLD shell cellulose $13.65{\cdot}10^{10}$ cm^{-2} for our data treatment we simplified the model by removing the shell component. We note that in this paper we adhere to the definition of microfibril in previous work (Martinez-Sanz et al. (Martínez-Sanz, Mikkelsen, Flanagan, Gidley, et al., 2016; Martínez-Sanz, Mikkelsen, Flanagan, Rehm, et al., 2016).), i.e. an entity with a diameter of 3-4 nm

2.5. Rheo-MRI

Time-averaged velocity profiles were measured according to procedures by Callaghan et al. (Callaghan, 1995, 1999) on a Bruker Avance II spectrometer at 7.0 T magnetic field strength (resonance frequency 300 MHz for ^1H). The magnet was equipped with a Bruker rheo-MRI accessory in combination with a cone-plate (CP) geometry made of PEEK (cone angle 7.0°, cone diameter 1 cm and 1.5% stress variation). For all imaging experiments, the field of view was set to 25 mm and profiles of 1024 points were collected, resulting in a spatial resolution of 24 μm. For each shear rate, 64 signal acquisitions were collected and averaged. All velocity profiles were corrected for slippage as described previously in (de Kort et al., 2016). For all measurements, a pre-shear at 80 s^{-1} was applied for 2 minutes.

3. Results and discussion

3.1. Microstructural properties

In a first instance, the structural properties of citrus fiber suspensions were studied both before and after HPH treatment. Whereas the rheological changes caused by HPH have been previously addressed by multiple studies (Benhamou, Dufresne, Magnin, Mortha, & Kaddami, 2014; Björkman, 2006; Grüneberger et al., 2014; Iotti, Gregersen, Moe, & Lenes, 2011; Karppinen et al., 2012b; Saarikoski et al., 2012; Saarinen, Lille, & Seppälä, 2009; Taheri & Samyn, 2016), its effect on cellulose multiscale structure is still unclear. Confocal images of a 1% wt. citrus fiber dispersion at different homogenisation pressures are shown in Fig. 1, where cellulose content is presented in black. Obtained results

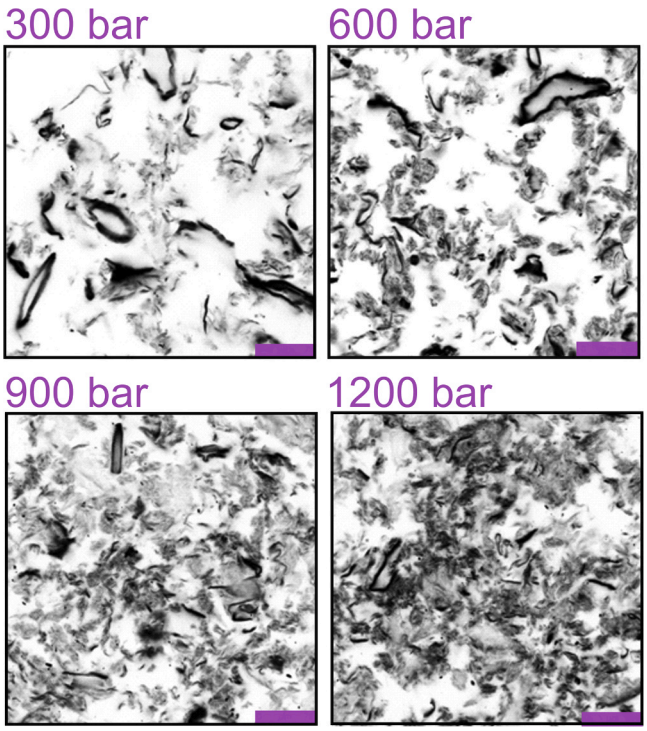

Fig. 1. Confocal images of a MNFC citrus fiber suspensions after high-pressure treatment at different pressure values. Scale bar corresponds to 75 μm. In all images white background represents the absence of cellulose fibrils.

clearly indicate that the microstructure of the cellulose dispersions is affected by mechanical pressure. After HPH treatment at low pressure values (300 bar) the recognized fiber strucures correspond to distrupted cell walls. High homogenization pressures, however, induces a disruption of the micron scale fibers and a more homogenous microstructure is obtained, as can be cleary observed at 1200 bars in Fig. 1 (Willemsen et al., 2020).

To gain structural information at a smaller length scale, we performed SAXS measurements on citrus fiber dispersions before and after HPH treatment for up to 4 passes through the homogenizer at 1200 bar. The peak maxima of Porod ($I(q)q^4$ vs q) and Kratky ($I(q)q^2$ vs q) plots revealed two dimensions, an invariable one near 3 nm (dimension A) and one near 10 nm (dimension B) that varied with HPH treatment (Fig. S2 in Supplementary Material). These dimensions were derived from the peak maxima in the Porod and Kratky plot, using the relationship d= 2π/q (where q is in nm^{-1}). While, the shorter dimension was attributed to a short range microfibrillar average packing distance, the longer dimension was associated to a long inter-microfibrillar average packing distance. Dimension B increased with number of HPH passes (Fig. 2a) and indicated that the packing of the microfibrils loosened. SAXS scattering curves for a 1% wt. citrus fiber dispersion were fitted using Eq.1 listed in the method section. This model assumes a cylinder form-factor model for the cellulose microfibrils, while a power-law function accounts for the agglomerates of the network. Although most works employing the core-shell cylinder model focused on the characterization of the individual microfibrils (Martínez-Sanz, Lopez-Sanchez, Gidley, & Gilbert, 2015; Martínez-Sanz, Pettolino, Flanagan, Gidley, & Gilbert, 2017; Martínez-Sanz, Gidley, & Gilbert, 2016; Martínez-Sanz, Mikkelsen, Flanagan, Gidley, et al., 2016), the power-law term contribution plays an important role in the description of the fibrillar network. The obtained fitted parameters (Table 1 in Supplementary Material) suggest that even though HPH treatment results in defibrillation of citrus fiber dispersions with elementary core radius R_{cyl}^{+} in order of 1.5 nm, multiple passes through the homogenizer mainly affects the fibrillar network described by the power law term. In scattering theory (Teixeira, 1988)

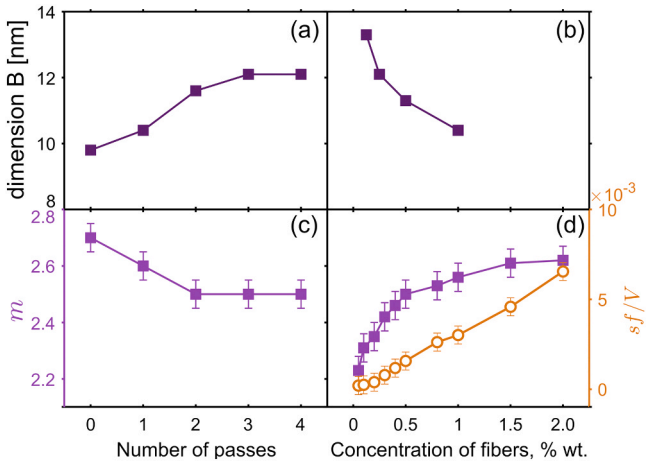

Fig. 2. Effect of HPH treatment and fiber concentration on structural parameters of citrus fiber dispersions as obtained by SAXS. (a,b) Kratky plot dimension B as a function of (a) number of HPH passes on a 1%wt. citrus fiber dispersion and (b) the concentration of citrus fibers. (c,d) Fitted structure power-law exponent m associated to mass fractal behavior as a function of (c) number of HPH passes on a 1%wt. citrus fiber dispersion and (d) the concentration of citrus fibers. In plot d also fitted volume fraction (sf/V) is presented. (right axis).

the power-law contribution is attributed to mass-fractal behavior: for $m < 3$ the fractal dimension D_f is given by $D_f = m$, while higher values of m correspond to higher density of fractal building blocks (Beaucage, 1996). Fig. 2c shows that m decreases with defibrillation and levels off at a value of 2.5 after 3 cycles. The latter effect suggests that, even though HPH treatment does not affect cross-sectional sizes of microfibrils in the sample, it disrupts their short-range order as well as the long range microfibrillar network leading to a decline in the network mass-fractal dimension D_f.

The effect of concentration of fibers on the structure of citrus fiber dispersions was also addressed by SAXS measurements. The longer dimension that could be derived from the Kratky plot decreased from 14 to 10 nm with concentration (Fig. 2b). This indicated that at low concentrations the HPH treatment resulted in more loss of packing order of the cellulose microfibrils.

Fig. 2d shows concentration variations of fitted power-law exponent m and the volume fraction sf/V. The obtained results show that both sf/V and power-law exponent m increase with fiber concentration. These observations can be explained by an increase in the density of fibers followed by a decrease in the distance between network nodes.

3.2. Flow behavior of HPH treated citrus fiber suspensions

The rheological behavior of homogenized citrus fiber dispersions was addressed by performing upward and downward sweep rate tests at different fiber concentrations (Fig. 3). We first note that the viscosity of the citrus fiber dispersions increases with the concentration of fibers, while a strong shear thinning behavior is observed for all samples. Similar behavior upon fiber concentration was also found in many microfibrillated cellulose dispersions (Nechyporchuk et al., 2016).

A peculiar feature of up-and-down flow curves in Fig.3 is the observed hysteresis in the low shear rate region. The latter effect indicates the presence of thixotropic yield stress behavior, and has been commonly associated to shear-induced changes in microfibril flocs shape and/or size (Nechyporchuk et al., 2016). Viscosity curves in Fig.3 also display a distinctive change of slope, or kink, at intermediate shear rate values (2 – 10 s^{-1}). Comparable observations were reported by Facchine et al. for Sodium-form defibrillated cellulose dispersions in a plate-plate geometry, relating this kink to a transition from anisotropic to isotropic floc microstructure (Facchine, Spontak, Rojas, & Khan,

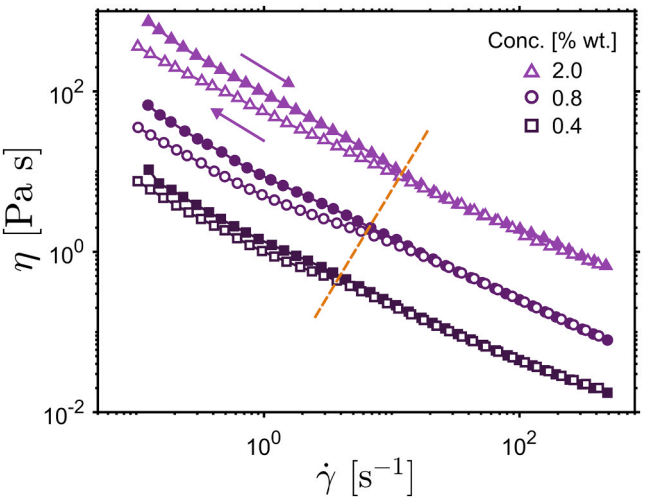

Fig. 3. Upward (filled symbols) and downward (empty symbols) shear rate sweep tests of MNFC citrus fiber suspensions at different fiber concentrations (0.4 – 2.0% wt.). Dashed line indicates the change in slope at intermediate shear rate values (2 – 10 s^{-1}).

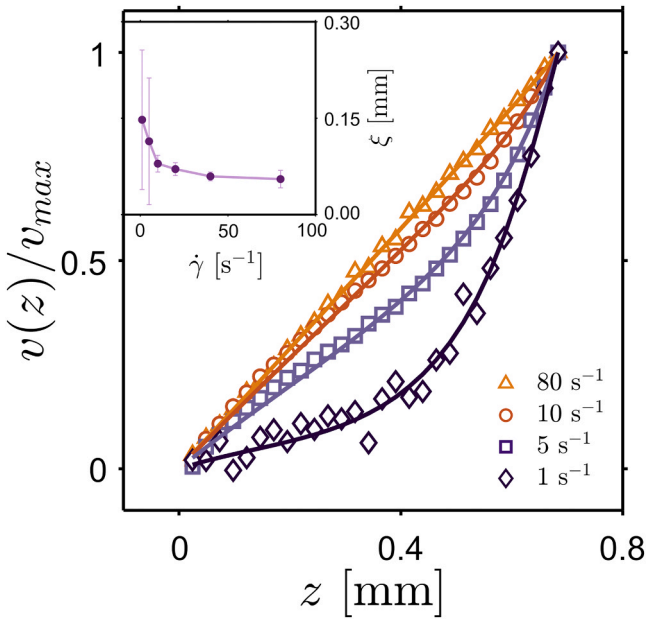

Fig. 4. Normalized rheo-MRI velocity profiles (symbols) of 0.3% wt. HPH-treated citrus fiber dispersion in a cone-and-plate geometry corrected for slip velocity at the plate, and fitting profiles (solid lines) using the non-local fluidity model described in (Serial, Maria et al., 2021) at different applied shear rates.

2020). Due to the beam orientation, no conclusion could be made on alignment along the vortex direction (Facchine et al., 2020). Interestingly, our results show (i) evidence that hysteresis increases with increasing fiber concentration, and (ii) the shear rate at which flow curves change in slope (see dashed line in Fig. 3). This last effect might be related to a stronger cellulose network at higher fiber concentrations, therefore requiring a higher shear rate value to disrupt anisotropic floc structure.

Given their inherent thixotropic properties, cellulose dispersions are also prone to exhibit flow localization or shear-banding, leading to the formation of regions of different viscosity and thus flow properties. To gain insight on flocculation dynamics of citrus fiber cellulose dispersions during shear, rheo-MRI measurements were performed in a 7° cone-and-plate geometry at increasing shear rates. In an homogenous stress field, velocity profiles for thixotropic yield stress fluids, are expected to be linear (constant local shear rate) at imposed shear rates above a critical value $\dot{\gamma}_c$ (Møller, Mewis, & Bonn, 2006; Møller, Rodts, Michels, & Bonn, 2008). Instead, if a shear rate below $\dot{\gamma}_c$ is applied, shear-banding is expected.

Fig. 4 shows local average velocities for a 0.3% wt. HPH-treated citrus fiber cellulose dispersion at increasing applied shear rates $\dot{\gamma}$. As observed, flow profiles are homogenous for $\dot{\gamma} > 10\ s^{-1}$, while rather curved profiles are encountered for $\dot{\gamma} < 10\ s^{-1}$, whereas discrete bands are expected for thixotropic fluids. Since the local viscosity $\eta(z)$ is given by $\eta(z) = \sigma_0/\dot{\gamma}(z)$, where z is the position along the gap, σ_0 is the nearly z-independent stress, and the local shear rate in a cone-and-plate geometry is $\dot{\gamma}(z) = \partial v(z)/\partial z$, the deviation from the expected flow behavior for thixotropic fluids suggests that viscosity varies spatially across the gap. Recently, Serial et al. (Serial, Maria et al., 2021) studied the effect of confinement in the flow behavior of a thixotropic microgel dispersion in a cone-and-plate geometry. Under such conditions, shear banding and cooperativity effects can coexist, resulting in curved velocity profiles and, therefore, in spatially-dependent local viscosities. Cooperativity effects have been observed in many particulate materials when the size of the fluid confinement is comparable to the length scale of the sample microstructure (Dijksman, 2019; Geraud, Bocquet, & Barentin, 2013; Goyon, Colin, Ovarlez, Ajdari, & Bocquet, 2008; Kamrin, 2019). In such situations, plastic rearrangements of particles during flow induce further rearrangements at distant locations, making the flow cooperative. This effect can be quantified by fitting the velocity profiles employing a non-local fluidity model (Goyon et al., 2008), which introduces a length scale ξ that accounts for the correlation length between plastic rearrangements. Commonly, ξ is expected to be on the same order of the particle size diameter of the material. The model proposed by Serial et al. (Serial, Maria et al., 2021) also allows to fit a critical shear rate $\dot{\gamma}_c$ below which shear banding effects influence the flow behavior of the dispersions.

In order to assess the non-local flow behavior of the citrus fiber cellulose dispersions, velocity profiles were analyzed using the model described in (Serial, Maria et al., 2021). For all velocity profiles, the critical value $\dot{\gamma}_c$ was considered as a global fitting parameter. The shear rate at the plate $\dot{\gamma}_{z=0}$ as well as the shear rate at the cone $\dot{\gamma}_{z=h}$ were taken as fixed fitting parameters. Fig. 4 displays fitted velocities employed the model described in (Serial, Maria et al., 2021) to describe cooperativity effects in strongly confined thixotropic materials, from which a critical shear rate $\dot{\gamma}_c = (1.5 \pm 1)\ s^{-1}$ and shear-dependent ξ can be obtained. Inset in Fig.4 shows that fitted ξ-values slightly decrease with increasing applied shear rate, obtaining an average length scale of $\xi = (0.09 \pm 0.02)$ mm. Similar observations were reported by de Kort et al. for bacterial microfibrillated cellulose dispersions in comparable cone-and-plate geometry, however the presence of shear banding due to the existence of a critical stress was not taken into account by the model (de Kort et al., 2016). Several authors have reported the presence of floc structures in the range of (100 – 300 μm) in cellulose dispersions produced using mechanical fibrillation (Karppinen *et al.* 2012a; Saarikoski et al., 2012). The length scale of these heterogeneities is comparable to the fitted ξ-values, as expected by the fluidity model. As described in Section 3.2, changes in size and orientation of microfibril flocs are usually associated as the main cause of hysteresis in microfibril cellulose dispersions (Facchine et al., 2020). At the same time, flow cooperativity has proven to be a complex phenomenon, commonly influenced by many factors such as particle dimensions and orientation, as well as sample heterogeneities and interaction between particles (de Cagny, Fall, Denn, & Bonn, 2015; Rajaram & Mohraz, 2012; van de Laar, Schroën, & Sprakel, 2015). The latter could explain the observed changes in the rheo-MRI flow behaviour at low shear rates, were cooperativity seems to be more pronounced and hysteresis start to take place as seen in Fig. 3

Our results show that confinement effects should be considered when characterizing the flow properties of thixotropic cellulose dispersions,

especially in such cases where floc sizes are comparable to the gap size of the geometry. However, further research is needed in order to assess whether cooperative effects are affected or triggered by the orientation and/or size of microfibril flocs along the vortex, as well as the impact of flow confinement on the obtained flow microstructure.

4. Conclusions

We have studied the microstructural and flow properties of HPH treated citrus fiber cellulose dispersions. The large shear applied on citrus fiber dispersions during HPH treatment does not affect cross-sectional sizes of the microfibrils in the system but does disrupt their short range order. On a larger scale, HPH treatment disrupts the microfibrillar network within intact microscale citrus fibers, the formation of a more space filling network is reflected in a decrease of the mass-fractal dimension as observed by SAXS. Under moderate shearing conditions (0,1-100 s^{-1}), cellulose citrus fiber dispersions display shear-thinning and thixotropic properties, as previously observed in similar samples at comparable concentrations. Localized flow measurements carried out in a cone-and-plate geometry show that thixotropic flow behavior is accompanied by non-local cooperative colloidal interactions, with a correlation length scale $\xi \sim 100\ \mu$m, which is in line with estimates for floc sizes for microfibrillated cellulose dispersions at similar applied shear rates.

Declaration of Competing Interest

J.P.M.v.D and R.d.A are employed by a company that markets products containing citrus fibers.

Acknowledgement/Funding

This work was part of the SSCANFOODS (project number 13386) and Hybrid Soft Materials programs, both financed by The Netherlands Organization for Scientific Research (NWO). C.T. acknowledges funding from the 4TU Precision Medicine program supported by High Tech for a Sustainable Future (https://www.4tu.nl/en/news/!/393/awarding_highteh/).

Appendix A. Supporting information

Supplementary data associated with this article can be found in the online version at doi:10.1016/j.foostr.2021.100237.

References

Alemdar, A., & Sain, M. (2008). Biocomposites from wheat straw nanofibers: Morphology, thermal and mechanical properties. *Composites Science and Technology, 68*(2), 557–565. https://doi.org/10.1016/j.compscitech.2007.05.044

Beaucage, G. (1996). Small-angle scattering from polymeric mass fractals of arbitrary mass-fractal dimension. *Journal of Applied Crystallography, 29*(2), 134–146. https://doi.org/10.1107/S0021889895011605

Benhamou, K., Dufresne, A., Magnin, A., Mortha, G., & Kaddami, H. (2014). Control of size and viscoelastic properties of nanofibrillated cellulose from palm tree by varying the TEMPO-mediated oxidation time. *Carbohydrate Polymers, 99*, 74–83. https://doi.org/10.1016/j.carbpol.2013.08.032

Björkman, U. (2006). The metarheology of crowded fibre suspensions. *Annual Transactions of the Nordic Rheology Society, 14*, 69–78.

Callaghan, P. T. (1995). Pulsed-gradient spin-echo NMR for planar, cylindrical, and spherical pores under conditions of wall relaxation. *Journal of Magnetic Resonance, Series A* (Vol. 113,(Issue 1), 53–59. https://doi.org/10.1006/jmra.1995.1055

Callaghan, P. T. (1999). Rheo-NMR: Nuclear magnetic resonance and the rheology of complex fluids. *Reports on Progress in Physics, 62*(4), 599–668. https://doi.org/10.1088/0034-4885/62/4/003

de Cagny, H., Fall, A., Denn, M. M., & Bonn, D. (2015). Local rheology of suspensions and dry granular materials. *Journal of Rheology, 59*(4), 957–969. https://doi.org/10.1122/1.4919970

de Kort, D. W., Veen, S. J., Van As, H., Bonn, D., Velikov, K. P., & Van Duynhoven, J. P. M. (2016). Yielding and flow of cellulose microfibril dispersions in the presence of a charged polymer. *Soft Matter, 12*(21), 4739–4744. https://doi.org/10.1039/c5sm02869h

Dijksman, J. A. (2019). Connecting the drops: observing collective flow behavior in emulsions. *Frontiers in Physics, 7*(November), 1–8. https://doi.org/10.3389/fphy.2019.00198

Doucet, M., Cho, J. H., Alina, G., Bakker, J., Bouwman, W., Butler, P., & Washington, A. (2018). *SasView version 4.2.*. https://doi.org/10.5281/zenodo.1412041

Dufresne, A., Dupeyre, D., & Vignon, M. R. (2000). Cellulose microfibrils from potato tuber cells: processing and characterization of starch-cellulose microfibril composites. *Journal of Applied Polymer Science, 76*(14), 2080–2092. https://doi.org/10.1002/(SICI)1097-4628(20000628)76:14<2080::AID-APP12>3.0.CO;2-U

Facchine, E. G., Spontak, R. J., Rojas, O. J., & Khan, S. A. (2020). Shear-dependent structures of flocculated micro/nanofibrillated cellulose (MNFC) in aqueous suspensions. *Biomacromolecules, 21*(9), 3561–3570. https://doi.org/10.1021/acs.biomac.0c00586

Geraud, B., Bocquet, L., & Barentin, C. (2013). Confined flows of a polymer microgel. *European Physical Journal E, 36*(3), 30. https://doi.org/10.1140/epje/i2013-13030-3

Goyon, J., Colin, A., Ovarlez, G., Ajdari, A., & Bocquet, L. (2008). Spatial cooperativity in soft glassy flows. *Nature, 454*(7200), 84–87. https://doi.org/10.1038/nature07026

Grüneberger, F., Künniger, T., Zimmermann, T., & Arnold, M. (2014). Rheology of nanofibrillated cellulose/acrylate systems for coating applications. *Cellulose, 21*(3), 1313–1326. https://doi.org/10.1007/s10570-014-0248-9

Iotti, M., Gregersen, Ø. W., Moe, S., & Lenes, M. (2011). Rheological studies of microfibrillar cellulose water dispersions. *Journal of Polymers and the Environment, 19*(1), 137–145. https://doi.org/10.1007/s10924-010-0248-2

Kamrin, K. (2019). *Non-locality in Granular Flow: Phenomenology and Modeling Approaches, 7*(August), 1–7. https://doi.org/10.3389/fphy.2019.00116

Karppinen, A., Saarinen, T., Salmela, J., Laukkanen, A., Nuopponen, M., & Seppälä, J. (2012a). Flocculation of microfibrillated cellulose in shear flow. *Cellulose, 19*(6), 1807–1819. https://doi.org/10.1007/s10570-012-9766-5

Karppinen, A., Saarinen, T., Salmela, J., Laukkanen, A., Nuopponen, M., & Seppälä, J. (2012b). Flocculation of microfibrillated cellulose in shear flow. *Cellulose, 19*(6), 1807–1819. https://doi.org/10.1007/s10570-012-9766-5

Klemm, D., Cranston, E. D., Fischer, D., Gama, M., Kedzior, S. A., Kralisch, D., & Rauchfuß, F. (2018). Nanocellulose as a natural source for groundbreaking applications in materials science: Today's state. *Materials Today, 21*(7), 720–748. https://doi.org/10.1016/j.mattod.2018.02.001

Martínez-Sanz, M., Gidley, M. J., & Gilbert, E. P. (2016). Hierarchical architecture of bacterial cellulose and composite plant cell wall polysaccharide hydrogels using small angle neutron scattering. *Soft Matter, 12*(5), 1534–1549. https://doi.org/10.1039/C5SM02085A

Martínez-Sanz, M., Lopez-Sanchez, P., Gidley, M. J., & Gilbert, E. P. (2015). Evidence for differential interaction mechanism of plant cell wall matrix polysaccharides in hierarchically-structured bacterial cellulose. *Cellulose, 22*(3), 1541–1563. https://doi.org/10.1007/s10570-015-0614-2

Martínez-Sanz, M., Mikkelsen, D., Flanagan, B., Gidley, M. J., & Gilbert, E. P. (2016). Multi-scale model for the hierarchical architecture of native cellulose hydrogels. *Carbohydrate Polymers, 147*, 542–555. https://doi.org/10.1016/j.carbpol.2016.03.098

Martínez-Sanz, M., Mikkelsen, D., Flanagan, B. M., Rehm, C., de Campo, L., Gidley, M. J., & Gilbert, E. P. (2016). Investigation of the micro- and nano-scale architecture of cellulose hydrogels with plant cell wall polysaccharides: A combined USANS/SANS study. *Polymer, 105*, 449–460. https://doi.org/10.1016/j.polymer.2016.07.015

Martínez-Sanz, M., Pettolino, F., Flanagan, B., Gidley, M. J., & Gilbert, E. P. (2017). Structure of cellulose microfibrils in mature cotton fibres. *Carbohydrate Polymers, 175*, 450–463. https://doi.org/10.1016/j.carbpol.2017.07.090

Martoïa, F., Perge, C., Dumont, P. J. J., Orgéas, L., Fardin, M. A., Manneville, S., & Belgacem, M. N. (2015). Heterogeneous flow kinematics of cellulose nanofibril suspensions under shear. *Soft Matter, 11*(24), 4742–4755. https://doi.org/10.1039/C5SM00530B

Møller, P. C. F., Mewis, J., & Bonn, D. (2006). Yield stress and thixotropy: On the difficulty of measuring yield stresses in practice. *Soft Matter, 2*(4), 274–283. https://doi.org/10.1039/b517840a

Møller, P. C. F., Rodts, S., Michels, M. A. J., & Bonn, D. (2008). Shear banding and yield stress in soft glassy materials. *Physical Review E - Statistical, Nonlinear, and Soft Matter Physics, 77*(4), Article 041507. https://doi.org/10.1103/PhysRevE.77.041507

Narayanan, T., Diat, O., & Bösecke, P. (2001). SAXS and USAXS on the high brilliance beamline at the ESRF. *Nuclear Instruments and Methods in Physics Research Section A: Accelerators, Spectrometers, Detectors and Associated Equipment, 467–468*, 1005–1009. https://doi.org/10.1016/S0168-9002(01)00553-8

Naz, S., Ahmad, N., Akhtar, J., Ahmad, N. M., Ali, A., & Zia, M. (2016). Management of citrus waste by switching in the production of nanocellulose. *IET Nanobiotechnology, 10*(6), 395–399. https://doi.org/10.1049/iet-nbt.2015.0116

Nechyporchuk, O., Belgacem, M. N., & Pignon, F. (2016). Current progress in rheology of cellulose nanofibril suspensions. *Biomacromolecules, 6*, Article b00668. https://doi.org/10.1021/acs.biomac.6b00668

Pennells, J., Godwin, I. D., Amiralian, N., & Martin, D. J. (2020). Trends in the production of cellulose nanofibers from non-wood sources. *Cellulose, 27*(2), 575–593. https://doi.org/10.1007/s10570-019-02828-9

Rajaram, B., & Mohraz, A. (2012). Steady shear microstructure in dilute colloid-polymer mixtures. *Soft Matter, 8*(29), 7699–7707. https://doi.org/10.1039/c2sm25936b

Yu, S., Sun, J., Shi, Y., Wang, Q., Wu, J., & Liu, J. (2021). Nanocellulose from various biomass wastes: its preparation and potential usages towards the high value-added products. *Environmental Science and Ecotechnology, 5*, 10077. https://doi.org/10.1016/j.ese.2020.100077

Saarikoski, E., Saarinen, T., Salmela, J., & Seppälä, J. (2012). Flocculated flow of microfibrillated cellulose water suspensions: An imaging approach for

characterisation of rheological behaviour. *Cellulose, 19*(3), 647–659. https://doi.org/10.1007/s10570-012-9661-0

Saarinen, T., Lille, M., & Seppälä, J. (2009). Technical aspects on rheological characterization of microfibrillar. *Cellulose Water Suspensions. Annual Transaction of the Nordic Rheology Society, 17*, 121–128.

Serial, M. R. (2021). High-pressure homogenized citrus fiber cellulose dispersions: structural characterization and flow behavior. *Online Presentation on Zenodo*. https://doi.org/10.5281/zenodo.5068052

Serial, Maria, R., Bonn, D., Huppertz, T., Dijksman, J. A., Van Der Gucht, J., van Duynhoven, J. P. M., & Terenzi, C. (2021). Non-local effects in the shear banding of a thixotropic yield stress fluid. *ArXiv E-Prints*.

Spence, K. L., Venditti, R. A., Rojas, O. J., Habibi, Y., & Pawlak, J. J. (2010). The effect of chemical composition on microfibrillar cellulose films from wood pulps: water interactions and physical properties for packaging applications. *Cellulose, 17*(4), 835–848. https://doi.org/10.1007/s10570-010-9424-8

Taheri, H., & Samyn, P. (2016). Effect of homogenization (microfluidization) process parameters in mechanical production of micro- and nanofibrillated cellulose on its rheological and morphological properties. *Cellulose, 23*(2), 1221–1238. https://doi.org/10.1007/s10570-016-0866-5

Teixeira, J. (1988). Small-angle scattering by fractal systems. *Journal of Applied Crystallography, 21*(6), 781–785. https://doi.org/10.1107/S0021889888000263

Van Buggenhout, S., Wallecan, J., Christiaens, S., Debon, S. J. J., Desmet, C., Van Loey, A., & Mazoyer, J. (2015). Influence of high-pressure homogenization on functional properties of orange pulp. *Innovative Food Science and Emerging Technologies, 30*, 51–60. https://doi.org/10.1016/j.ifset.2015.05.004

van de Laar, T., Schroën, K., & Sprakel, J. (2015). Cooperativity and segregation in confined flows of soft binary glasses. *Physical Review E, 92*(2), Article 022308. https://doi.org/10.1103/PhysRevE.92.022308

Willemsen, K. L. D. D., Panozzo, A., Moelants, K., Debon, S. J. J., Desmet, C., Cardinaels, R., & Hendrickx, M. E. G. (2017). Physico-chemical and viscoelastic properties of high pressure homogenized lemon peel fiber fraction suspensions obtained after sequential pectin extraction. *Food Hydrocolloids, 72*, 358–371. https://doi.org/10.1016/j.foodhyd.2017.06.020

Willemsen, K. L. D. D., Panozzo, A., Moelants, K., Wallecan, J., & Hendrickx, M. (2020). Towards improved understanding of the viscoelastic properties of functionalized lemon peel fibers in suspension based on microstructure, hydration value and swelling volume. *Journal of Food Engineering, 278*(January). https://doi.org/10.1016/j.jfoodeng.2020.109950

Zuluaga, R., Putaux, J. L., Cruz, J., Vélez, J., Mondragon, I., & Gañán, P. (2009). Cellulose microfibrils from banana rachis: Effect of alkaline treatments on structural and morphological features. *Carbohydrate Polymers, 76*(1), 51–59. https://doi.org/10.1016/j.carbpol.2008.09.024